Fiber-Optic Bragg Grating Sensor for Photothermally Examinating Moisture of Meat

Xiaodong XIE[1], Enlai SONG[1], Ziyu YUAN[1], Yi YIN[1], Yongkang ZHANG[1], Qiaochu YANG[1], Zhiyuan XU[2*], and Yang RAN[1,2*]

[1]*Guangdong Provincial Key Laboratory of Optical Fiber Sensing and Communications, Institute of Photonics Technology, Jinan University, Guangzhou 510632, China*

[2]*Clinical Laboratory Center, The Affiliated Guangdong Second Provincial General Hospital of Jinan University, Guangzhou 510317, China*

[*]Corresponding authors: Zhiyuan XU and Yang RAN E-mails: 2016jnuxzy@stu2018.jnu.edu.cn and tranyang@jnu.edu.cn

Abstract: The illegal water injection into meat not only breaks the market equity, but also deteriorates the meat quality and produces harmful substances. In this work, we proposed a fiber Bragg grating (FBG) sensor that enabled fast, quantitative, and in-situ detection of the moisture content of water-injected meat. The FBG was written in the erbium-ytterbium (Er/Yb) co-doped fiber, which could perform the self-photothermal effect by injecting the near infrared laser into the fiber. As the heated fiber sensor probe was inserted into the meat sample, the temperature decreased due to the heat dissipation mediated by moisture. The intracore Bragg grating could monitor the temperature loss by recording the Bragg wavelength shift, which reflected the water content quantitatively. The results revealed that the sensor could complete the detection within 15 s. The sensor's sensitivity to detect changes in the pork water content was theoretically calculated to be 0.090847%. The proposed sensor is expected to provide a novel approach for examination of the meat moisture.

Keywords: Optical fiber sensor; fiber Bragg grating; active fiber; photothermal effect; heat conduction; meat moisture

Citation: Xiaodong XIE, Enlai SONG, Ziyu YUAN, Yi YIN, Yongkang ZHANG, Qiaochu YANG, *et al.*, "Fiber-Optic Bragg Grating Sensor for Photothermally Examinating Moisture of Meat," *Photonic Sensors*, 2024, 14(3): 240310.

1. Introduction

Water-injected meat is a type of low-quality food that frequently appears in the meat market. The injected water increases up to 15%–20% of the net weight of meat for illegal profit [1]. In recent years, dishonest traders used chemical agents and drugs solutions that contained red dyes and gelatinous substances as additives. Red pigments can enhance the appearance of meat, making it look fresher. Gelatinous substances can retain moisture and prevent water from overflowing, resulting in the injected pork being indistinguishable from the normal pork [2]. Injecting water into meat not only disrupts the market order, but also poses a risk to human physical health [3, 4].

The continuous emergence of water-injected meat in the market has attracted widespread attention to the safety of meat products. As a result, the examination of water-injected meat has become a research hotspot. The traditional method uses manual inspection to determine whether meat has

Received: 10 August 2023 / Revised: 5 January 2024

DOI: 10.1007/s13320-024-0720-6
Article type: Regular

been injected [3–7]. However, due to individual differences in sensory perception, the judgment of each person may vary, leading to deterioration of detection accuracy.

Laboratory testing methods mainly include the microscopic examination, paper-based test, drying, drip loss, pressure test, and freezing [3, 7]. The drying method is adopted in the guideline of "Moisture Limits for Livestock and Poultry Meat" (GB 18394-2020, China). Although the measurement of meat moisture is accurate and reliable, the detection process is time-consuming and may compromise the integrity of the sample.

Researchers have proposed various non-destructive testing methods, such as harnessing sound, light, magnetism, and electricity to assess the water content of the meat sample [8–13]. The non-destructive test has significant advantages over traditional methods, including its non-destructive nature, comprehensive approach, ability to cover the entire process, and high reliability. However, non-destructive testing methods generally encounter the challenge of quantitative testing. Developing a rapid, quantitative, and in-situ detection method for the water content of injected meat is of significant practical importance.

The fiber Bragg grating (FBG) has been extensively researched and utilized in the field of optical sensing due to its exceptional advantages, such as compactness, resistance to electromagnetic interference, high sensitivity, and high speed. Current research indicates that FBG sensors can achieve rapid and accurate measurement of the water content by utilizing the photothermal effect of the doped fiber and the principle of FBG temperature measurement [14–21]. These sensors have demonstrated a significant development potential. Sun *et al*. [15] proposed an actively heated optical fiber method (AHFO) based on the quasi-distributed FBG (AHFO-FBG) technology for large-scale in-situ measurement of the soil moisture content. Wang *et al*. [17] developed an all-fiber sensor for measuring the micro soil moisture content, which allows for real-time in-situ monitoring of the soil moisture content with a maximum error of only 1.41%. Mehravar *et al*. [18] developed an FBG sensor embedded in a polymer optical fiber. It was able to detect small changes in the soil water content even as low as 0.5%.

The latest research indicated that the endogenous photothermal effect of active optical fibers could be utilized to conduct photothermal therapy on malignant tumors [22]. This presented a novel method for incorporating internal heat sources into FBG sensors for detecting the moisture content.

This work had explored the FBG sensor for detecting the moisture content of meat by orchestrating the endogenous photothermal effect of active optical fibers and the FBG temperature sensor. As the heated fiber sensor probe was deposited in the meat sample on site, the temperature would decrease caused by the heat dissipation in the moisture condition. The intracore Bragg grating could record the temperature decrease quantitatively, which reflected the water content in the meat sample. The results revealed that the sensor could finish a detection less than 15 s. The sensitivity of the sensor regarding the meat water content could be theoretically estimated to 0.090 847%. The proposed sensor is expected to provide a novel approach for examination of the meat moisture.

2. Principle and theory

2.1 Design of sensor probe

The sensor probe was fabricated using an erbium/ytterbium (Er/Yb) fiber with an FBG written in it. The Er/Yb fiber served as the self-heating element to generate heat through the photothermal effect, while the FBG functioned as the in-situ temperature sensor to detect the temperature drop of the Er/Yb fiber caused by moisture in pork, as shown in Fig. 1(a).

Firstly, a piece of Er/Yb fiber with a ~2 cm length was prepared and connected to a light source

and a spectral analyzer for real-time monitoring of the spectral evolution of the FBG. The FBG was fabricated using the phase mask method [23–25]. The 193 nm ultraviolet light emitted by an excimer laser (Coherent model: COMPexPro110) was used as the laser source. A phase mask with a wavelength of 1 065.51 nm was selected to set a suitable Bragg wavelength. The transmission spectrum of the fabricated FBG is shown in Fig. 1(b).

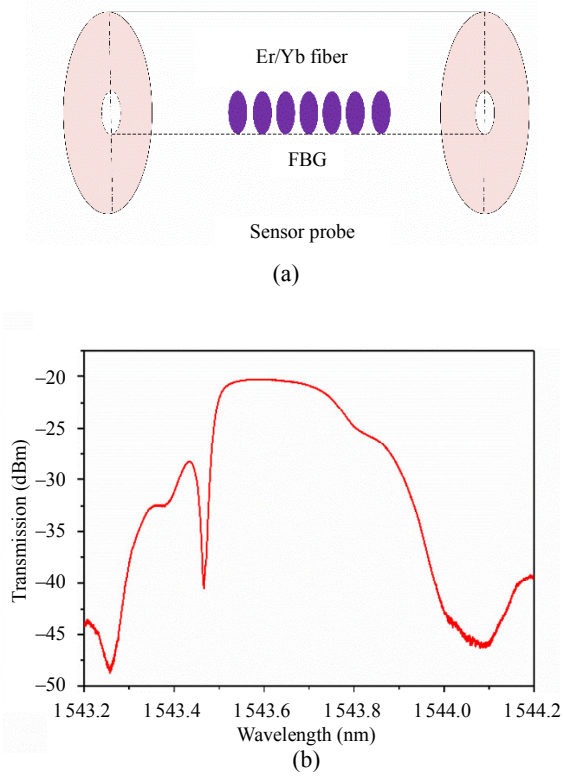

Fig. 1 Structure and spectrum of the sensor: (a) schematic of the fiber-optic probe using an FBG written in the Er/Yb fiber (the Er/Yb fiber serves as the self-heating element, while the FBG functions as the in-situ temperature sensor) and (b) transmission spectrum of the FBG in the fiber-optic sensor probe (when connecting the sensor to a broadband light source and spectrometer, the reflection spectrum can be observed).

2.2 Thermal effect of the sensor probe

The thermal conduction between optical fibers and the external environment, as well as the photothermal effect of optical fibers, can result in temperature variation within the fiber core. The change in temperature within the fiber can not only cause thermal expansion but also alter the refractive index of the fiber. Both of these effects can lead to a drift in the spectrum of the FBG. According to the Bragg conditions, we can derive the relationship between the temperature change in the fiber and the drift of the central wavelength of the Bragg grating:

$$\Delta\lambda = 2\left(\Lambda\frac{\partial n_{\text{eff}}}{\partial T} + n_{\text{eff}}\frac{\partial \Lambda}{\partial T}\right)\Delta T \tag{1}$$

where Λ is the period of the FBG, and n_{eff} is the effective refractive index of the fiber.

In the above equation, the right side illustrates the impact of temperature on FBGs. The thermal expansion resulting from an increase in temperature alters the refractive index and grating spacing, causing a shift in the wavelength of FBGs. This indicates that FBGs with the same period have identical temperature sensing characteristics.

To investigate the effects of temperature changes in the environment on the sensor probe, the probe was placed in a temperature-controlled box for heating. The study measured the correlation between air temperature changes and the drift of the FBG spectral peak. During the experiment, the indoor temperature was 24.6 ℃, and the temperature range of the selected temperature control box was 0 ℃–100 ℃. Firstly, the temperature of the incubator was raised to 80 ℃. Three sets of initial FBG spectra were recorded separately after the sensor and environmental temperature reached thermal equilibrium. The temperature box was then controlled to slowly reduce the internal temperature. Three sets of FBG spectra for every 2 ℃ decrease were recorded once thermal equilibrium was achieved.

Similarly, to investigate the effect of temperature variation in aquatic environments on the sensor probe, the probe was submerged in water and subjected to heating. The temperature of the heater was adjusted, which led to the water temperature increasing from 28 ℃ to 50 ℃. The temperature here should not exceed 50 ℃. If it did, bubbles might be generated, leading to strain disturbances and potentially affecting the accuracy of temperature detection. Nevertheless, this temperature range was sufficient

for our subsequent experiments. Three sets of FBG spectra for every 2 ℃ increase in temperature were recorded separately once the water and fiber temperatures had reached thermal equilibrium.

Based on the above experiment, we obtained the temperature response characteristics of the probe in both environments of air and water, as shown in Fig. 2.

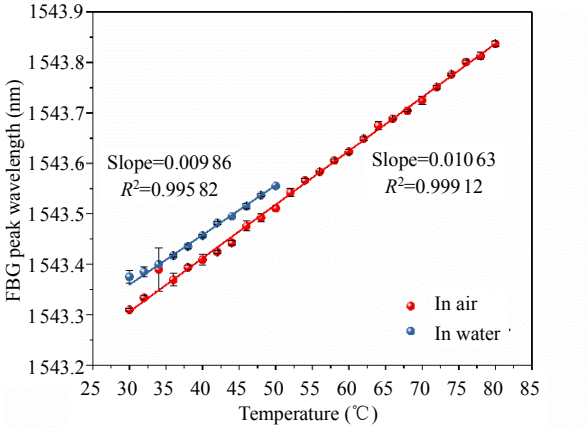

Fig. 2 Temperature response characteristics of the sensor probe in both environments of air and water.

Based on the linear regression analysis of the experimental data, the temperature sensitivity of the sensor probe in both environments of air and water could be determined, as presented in Table 1.

Table 1 Temperature response characteristics of the sensor probe.

Environment	Air	Water
Temperature sensitivity (nm/℃)	0.010 63	0.009 86

According to the table above, the temperature response characteristics of the sensor probe are almost the same in both environments of air and water, presenting the versatility of the sensor in different ambiences. This is due to the stable external environment temperature control, which results in the uniform grating responses.

As Er/Yb fiber was connected to 980 nm pump light, a portion of the energy from the LD laser was up-converted into green light emission and up-converted to the spontaneous emission photon energy, respectively. The remaining photonic energy was transformed into heat mediated by the non-radiative transition, leading to an increase in the temperature of the fiber core. The heat deposited in the fiber core was primarily transferred to the cladding through solid heat conduction, while the heat in the cladding continued to dissipate outward. This would reduce the temperature inside the fiber core, allowing it to reach thermal equilibrium and ultimately form a steady-state temperature field within the fiber.

To investigate the thermal impact of pump light on sensor probes, we positioned the pumped probes in both air and water conditions. The pump power was gradually increased from 0 mW to 500 mW with an increment of 25 mW. After 60 s, three sets of FBG spectra were recorded once the sensor probe had reached internal thermal equilibrium. The wavelength shifts of the sensor probe regarding both conditions are illustrated in Fig. 3.

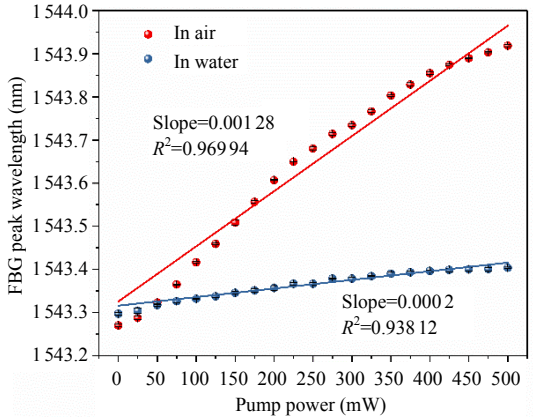

Fig. 3 Photothermal response characteristics of sensors in air and water conditions.

Based on the linear regression analysis of the experimental data, the temperature sensitivity of the sensor probe in both air and water conditions could be determined, as presented in Table 2.

Table 2 Pump light response characteristics of the sensor probe.

Environment	Air	Water
Temperature sensitivity (nm/℃)	0.001 28	0.000 2

At room temperature, the thermal conductivity of air is 2.552×10^{-2} W/(m·K), the specific heat

capacity is 1.013×10^3 J/(kg·K); The thermal conductivity of water is 0.574 W/(m·K), and its specific heat capacity is 4.2×10^3 J/(kg·℃). Because water has a higher thermal conductivity than air, heat transfer from the optical fiber to the external environment occurs more rapidly. In addition, water has a higher specific heat capacity than air, denoting that it can absorb more heat from optical fibers than the air. By taking into account the heat transfer from the fiber to the air following an increase in pump light power, we can derive the relationship between the pump light power and fiber temperature as follows:

$$T=\frac{0.001\ 28}{0.010\ 63}P+T_0 \tag{2}$$

where P is the pump light power, its unit is mW; T is the surface temperature of the optical fiber, T_0 is the initial temperature of the fiber surface, and their units are K.

3. Simulation

A solid and porous medium heat transfer model was established, to simulate the process of detecting the moisture content of the pork by using the sensor. When the pump light was turned on, the sensor generated thermal deposition through the photothermal effect of its active optical fiber part. This heat quantity was then transmitted to the fiber cladding, pork interior, and air environment through thermal conduction [26, 27]. This work was finished by the finite element analysis software.

3.1 Simulation of photo-thermal effect of the sensor probe

The photo-thermal effect model of sensor probes can be represented as follows [28, 29]:

$$q(r)=\begin{cases}\mu\cdot\alpha\cdot P(r,z) & (0<r\leqslant r_1)\\ 0 & (r_1<r\leqslant r_2)\end{cases} \tag{3}$$

where η is the thermal conversion efficiency, r_1 and r_2 are the radii of optical fiber core and cladding, respectively, α is the pump absorption coefficient, and $P(r,z)$ is the spatial distribution of the pump light in the active fiber, which can be expressed as

$$P(r,z)=P_0\cdot \mathrm{Pt}(r)\cdot\exp(-\alpha z) \tag{4}$$

where P_0 is the incident pump power, and $\mathrm{Pt}(r)$ is the normalized energy distribution of the optical fiber fundamental mode. Most rare-earth ions doped fibers are multimode at 980 nm. However, when the fusion loss between the active fiber and single-mode fiber is very small and without bending the optical fiber, the high-order mode part is very small.

During the simulation process, we simplified the model by assuming that the active optical fiber section of the probe was ~2 cm and nearly saturated. Without considering the temperature distribution along the axis of the probe, we simplified the model into a two-dimensional axisymmetric model. The optical field distribution of the basic mode transmitting in the optical fiber core is shown in Fig.4. The distribution closely approximated a Gaussian distribution, and based on the fitting curve results, the standard deviation (σ) was 2.545 48 μm.

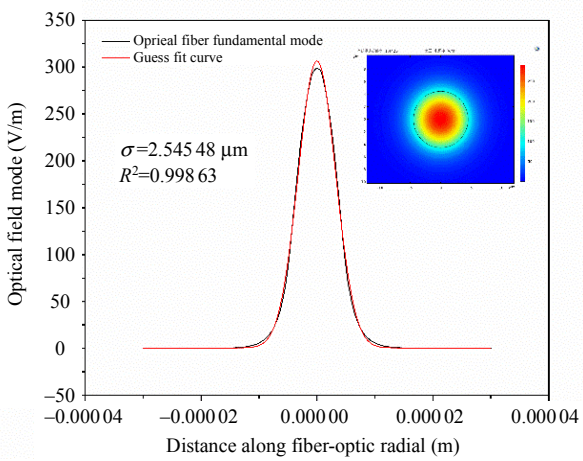

Fig. 4 Simulation of the heat source in the sensor probe. The self-heating energy of the Er/Yb fiber is related to the normalized energy distribution of the optical fiber fundamental mode.

To begin, we set the initial temperature of both the sensor probe and pork in the model to 297.75 K. With a pump power of 400 mW, the surface temperature of the optical fiber could be calculated to be 350.70 K by utilizing (2). Assuming that there was no airflow indoors during the experiment, convective heat transfer of air could be approximately ignored.

By the finite element analysis software, a heat transfer model was established between the optical fibers and air. The model approximated a solid heat transfer model without airflow. When setting the power parameter of the deposition beam in the debugging model as P_0 =5.5×10^{-6} W, the optical fiber surface in the model could reach 350.70 K. The heat source based on the model of the sensor probe is as follows:

$$P' = P_0' \cdot \frac{1}{2\pi\sigma^2} \cdot \exp\left(-\frac{r^2}{2\sigma^2}\right) \tag{5}$$

where P' is the simulated heat source thermal power, the deposited beam power is P_0'=5.5×10^{-6} W, and the standard deviation σ=2.545 48 μm.

3.2 Simulation of the pork moisture content detection experiment

The research subject of this experiment was the lean pork meat. Conventionally, the water content of the lean pork is 70%. The water present in the pork can be roughly divided into three types: bound water, non-flowing water, and free water, with proportions of 5%, 80%, and 15%, respectively. Bound water and non-flowing water exist within the cell interior and among the filaments, myofibrils, and membranes, respectively. Free water, on the other hand, exists in the extracellular space and can flow freely. The water injected into the pork is primarily in the form of free water. For this reason, the pork was simplified as a porous medium model, assuming that the water in the pores remained stationary.

By the finite element analysis software, a heat transfer model was established for the pork moisture content detection sensor. Firstly, "heat transfer – porous medium heat transfer" was selected as the physical field for research. Next, a geometric model was established that was center-symmetric for both the optical fiber and pork. From the center, the inner layer was solid, consisting of the optical fiber core and cladding, while the outer layer was a porous medium consisting of the water-injected pork. The radii of the fiber core and cladding were 4.5 μm and 62.5 μm, respectively, and the thickness of the outer porous medium was 2 cm.

Next, three layers of material were set up. The fiber core and cladding should be made of silica glass material, with the main parameters being C_p = 7 031 J/(kg·K), ρ = 2 203 kg/m^3, and k = 1.38 W/(m·K). The main parameters of water-injected pork were set as C_p = 3 432 J/(kg·K), ρ = 1 170 kg/m^3, and k = 0.455 W/(m·K), and porosity was calculated based on the volume ratio of free-flowing water to the meat matrix in the pork.

The initial temperature value for each part of the model should be 297.75 K. The outer boundary should be in contact with indoor air, with a constant boundary temperature of 297.75 K. The internal heat source should be the conversion of the active optical fiber photothermal effect, which could be set using (5). The specific parameters for this formula should be the deposited beam power P_0'=5.5×10^{-6} W and standard deviation σ=2.545 48 μm.

Finally, the model was meshed with an "ultra-fine" unit size. Additional research was conducted on the "frequency domain transient" by setting the output time from 0 s to 60 s with a step size of 0.1 s. After executing the calculation steps, the simulation results could be obtained. We selected the radial temperature field of the model at 0 s, 20 s, 40 s, and 60 s, and the corresponding simulation results are presented in Fig. 5.

Using the simulation model provided above, the amount of water injected into the pork was set at 0 mL, 0.5 mL, 1 mL, 1.5 mL, 2 mL, and 2.5 mL. A point on the cladding of the optical fiber was selected with coordinates (62.5 μm, 0 μm). The temperature at this point between 0 s and 60 s is displayed in Fig. 6(a). After turning on the pump light for 15 s, the temperature stabilized, indicating that the sensor had a response time of approximately 15 s. The relationship between the amount of water injection and the surface temperature of the sensor probe is depicted in Fig. 6(b). According to the heat

conduction equation, we believe that the numerical solution exhibited exponential correlation. This idea had been validated through the simulations above, in which the R^2 value for exponential curve fitting was 1. In subsequent experiments, we also adopted the exponential fitting method.

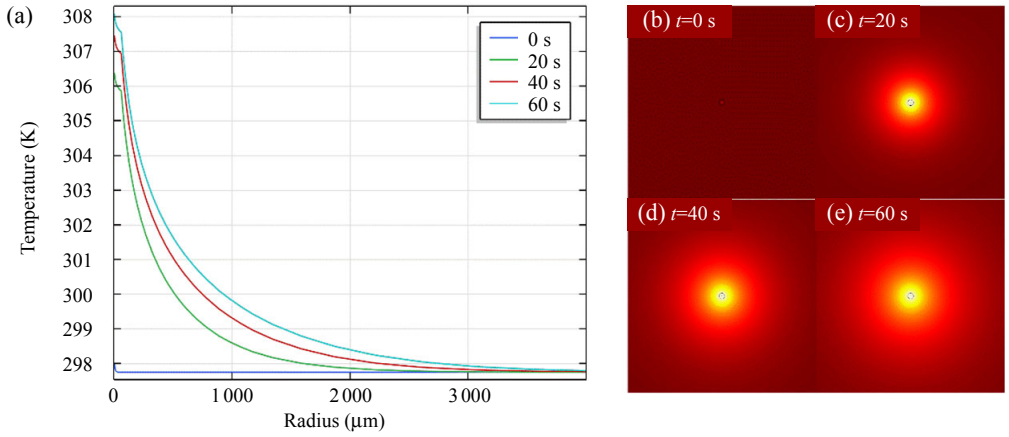

Fig. 5 Simulation of pork moisture content detection: (a) in the simulation, when the pump light with the power of 400 mW is turned on, the radial temperature distribution of the model is shown at 0 s, 20 s, 40 s, and 60 s. (b), (c), (d), and (e) are the temperature distributions of the model section at 0 s, 20 s, 40 s, and 60 s when the pump light with a power of 400 mW is turned on, respectively.

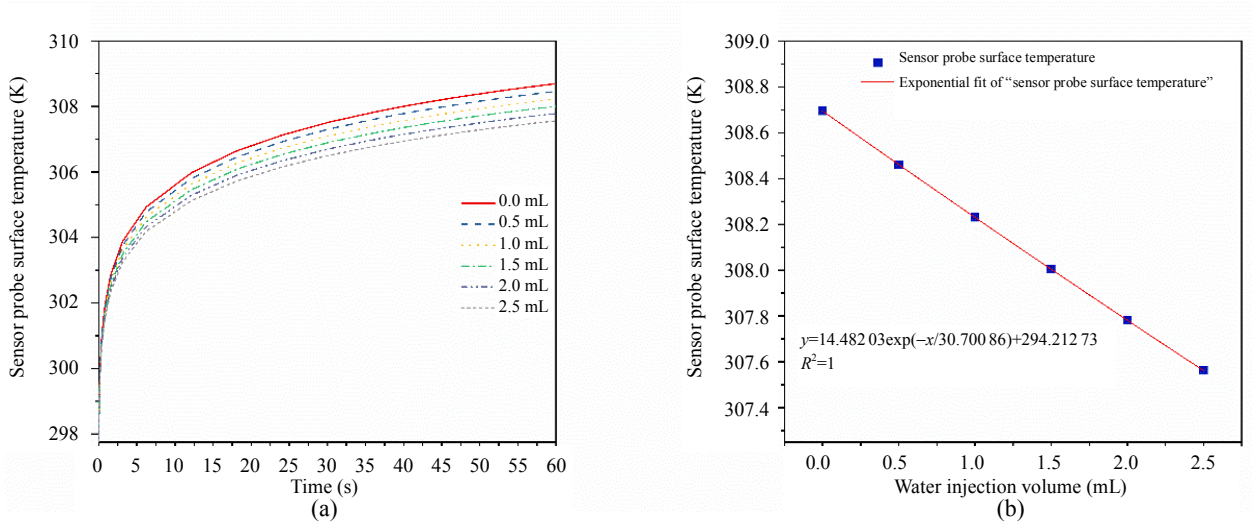

Fig. 6 Simulation results: (a) the surface temperature of the sensor probe record within 1 min with the water injection volume parameter set at 0 mL, 0.5 mL, 1 mL, 1.5 mL, 2 mL, and 2.5 mL, respectively (this indicates the fast response characteristic of the simulated sensor) and (b) the surface temperature of the optical fiber calculated at 60 s with the water injection volume parameter set as following values (this shows that the temperature of the optical fiber decreases with an increase in water injection, and an exponential curve is used to fit the simulated values).

4. Principle and theory

4.1 Detection system

The experimental setup for detecting the water content of pork tenderloin is illustrated in Fig. 7. The sensor probe was connected to the output end of the wavelength division multiplexer (WDM) using optical fiber cables. The two input ports of the WDM were connected to a pump light source with a wavelength of 980 nm and the 3 dB coupler. The 3 dB coupler was connected to a broadband light source and a high-resolution optical spectral analyzer (OSA), respectively. The actual detection system built in the laboratory is shown in Fig. 8.

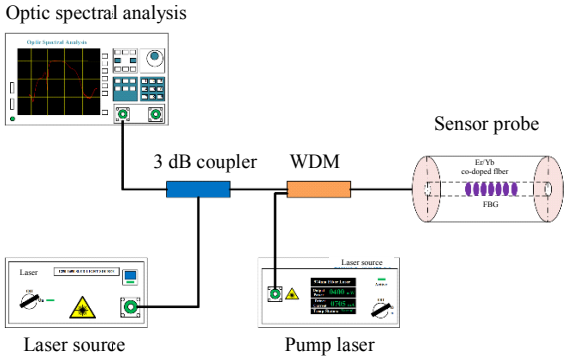

Fig. 7 Schematic diagram of the meat moisture content detection sensor system.

4.2 Detection system

In the experiment, we chose the lean pork as the experimental sample. According to relevant materials and literature, it was found that the main components of the pork are protein, fat, water, and a very small amount of trace elements. The fat content of meat does not have a significant effect on thermal conductivity. Instead, the ratio of protein to water content in meat affects thermal conductivity [30]. In addition, lean meats have a higher moisture content and can absorb more moisture compared with the fatty pork [31]. Therefore, the lean meat is the primary source of the water-injected meat in the market. We had chosen the lean pork as the subject of our research due to its representativeness.

A fresh piece of the lean pork with the weight of 66.7 g was prepared as the experimental sample. After a sufficient heat exchanging period within the laboratory environment, the pork's temperature was equivalent to the room temperature. The pork should be completely wrapped in dry cling film to prevent moisture loss.

After constructing the detection system, the sensor probe should be inserted into the pork at the appropriate depth to measure its internal moisture content. Because the optical fiber was fragile, the sensor probe could not be inserted directly into the pork. We needed to complete this operation using a syringe needle. Firstly, the sensor was inserted into the syringe needle and it must be concealed within the needle. Then, we inserted the syringe needle into the pork as deeply as possible, which protected the sensor probe. This ensured that the Bragg grating section of the optical fiber-doped sensor was fully immersed in the meat. Finally, we carefully removed the syringe needle and set it aside, away from the pork, to avoid any potential contamination or interference. Keeping it still for 10 min ensured that after the syringe needle was pulled out, the pork returned to its original shape and fit tightly against the sensor probe. As the pump laser in the system was turned on, the self-heating of the sensor caused its temperature to rise. The temperature of the sensor probe decreased due to the heat dissipation facilitated by moisture. The intracore Bragg grating could monitor temperature changes by recording the shift in the Bragg wavelength, which provided a quantitative measure of the water content.

Fig. 8 Detection of pork moisture content in laboratory: (a) actual detection system built in the laboratory, (b) sensor probe inserted into the pork sample, and (c) sensor probe with the pump light injected into it.

At the beginning of the experiment, the laboratory temperature was 24.6 ℃. The spectrum without injecting water into the pork was recorded as the baseline. Setting the power of the pump laser to 400 mW, the FBG spectrum was recorded immediately within 60 s after turning on the pump laser. The data were collected every 2.5 s. A total of 24 data sets were collected, which were completed

using the computer software connected to the OSA. Each time, we chose a fixed position directly above the sensor in the pork and slowly injected 0.5 mL of pure water into it by using a syringe. After each injection, waiting for 15 min ensured that the pork fully absorbed the water. Then, the FBG spectrums should be recorded within 60 s using the same method mentioned above once the pump was turned on. Immediately turning off the pump light source and waiting for 5 min to allow the pork to cool down to its initial temperature, we repeated the previous step twice. Until a total of 2.5 mL of water had been injected into the pork and water was observed seeping from the bottom of the pork inside the preservation film, we stopped injecting water and terminated the experiment.

After completing the experiment, we processed the collected spectral data to determine the correlation between the amount of injected water and the peak wavelength shift of the FBG reflection spectrum of the sensor, as shown in Figs. 9(a) and 9(b). Here, a specific portion of the FBG spectrum (near 1543.545 nm) was chosen to calibrate the spectral shift. Meanwhile, as shown in Fig. 9(c), the sensor responded within 15 s and then stabilized, indicating a sensor response time of 15 s.

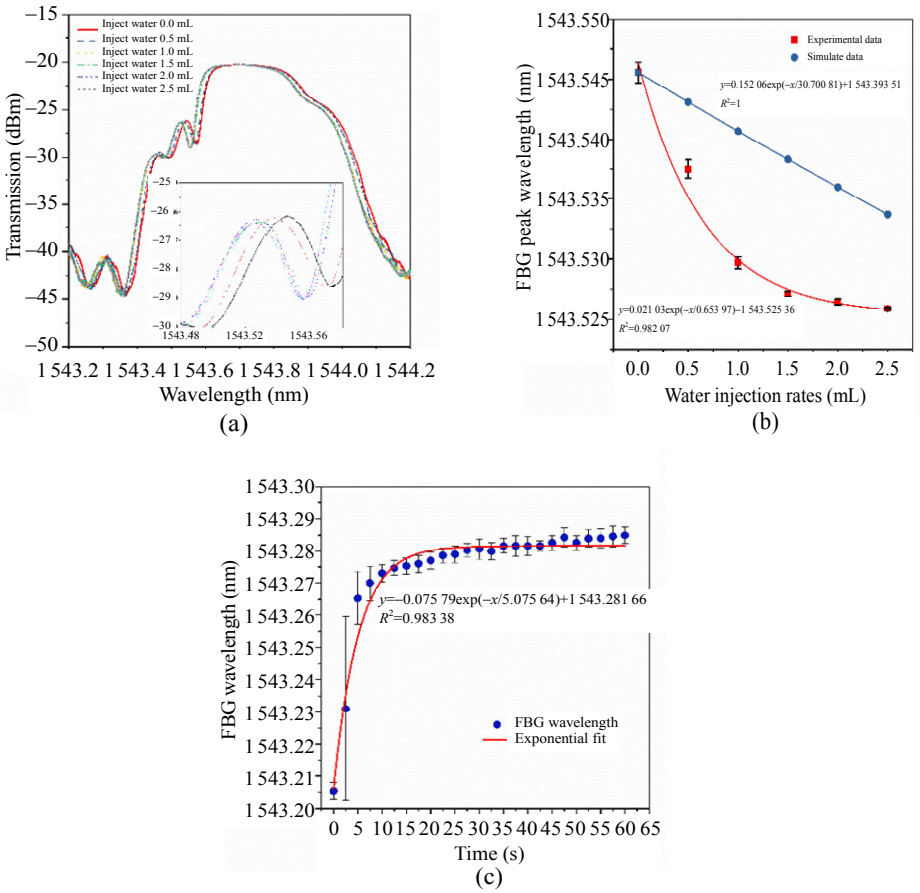

Fig. 9 Experimental results: (a) FBG peak wavelength shift process of the sensor in one of the repeated experiments with the water injection volumes of 0 mL, 0.5 mL, 1 mL, 1.5 mL, 2 mL, and 2.5 mL, respectively; (b) FBG peak wavelength of the sensor with the pork under various water injection rates (red dots and line: the FBG peak wavelength is measured when the water injection volume is 0 mL, 0.5 mL, 1 mL, 1.5 mL, 2 mL, and 2.5 mL, respectively, which reveals the corresponding relationship between the sensor FBG peak and water injection rates into the pork; blue dots and line: they are simulated data obtained through the following model established using the finite element software, which is used for comparison with experimental data; (c) time response characteristics of the sensor measured in the experiment.

4.3 Eliminate environmental temperature interference

FBGs are sensitive not only to the temperature of the fiber itself, but also to the ambient temperature. Changes in environmental temperature can also cause the drift in the grating peak, which may interfere with the detection results. Although the ambient temperature in the laboratory remains relatively constant, environmental temperature interference cannot be completely ignored during practical measurements. It can be challenging to maintain a consistent ambient temperature. Therefore, eliminating environmental temperature interference is a key issue that needs to be studied. This factor determines whether the sensor can be applied practically.

In previous research in related fields, Sun *et al*. [32] have proposed temperature compensation schemes by serializing a doped FBG front-end with a single-mode FBG. By using this method, we had improved our sensor probe. The doped optical fiber FBG part was completely embedded within the pork, while the single-mode FBG part was positioned on the surface of the pork to calibrate temperature, thereby achieving temperature compensation.

During the experiment, it was observed that the peak wavelength of the single-mode FBG increased from 1532.875 nm at 23 min to 1532.882 nm at 44 min during the fastest heating period, as shown in Fig. 10. Based on the earlier measurement of temperature sensitivity, it could be estimated that there was an increase of approximately 0.6648 ℃, with an average temperature rise of about 0.0317 ℃/min. The increase caused a wavelength drift of less than 0.00033 nm, which was lower than the resolution of the OSA, which was 0.001 nm. It could generally be believed that within 1 min of heating, the impact of ambient temperature could be disregarded.

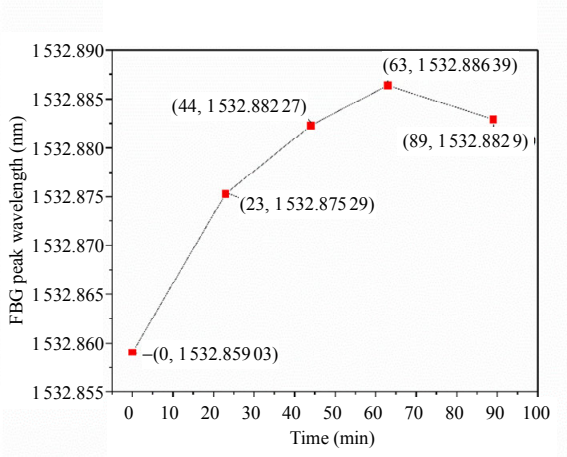

Fig. 10 Peak wavelength drift of the FBG in the single-mode fiber serves as a reference during the experimental process.

5. Analysis

In the simulation, assuming a pork mass of 66.7 g, an initial water content of 70%, and uniform absorption of injected water throughout the pork, the water injection is converted into the pork's water content. Simultaneously, the temperature response characteristic of the sensor is utilized to convert the temperature into the peak wavelength of the FBG. This enables the establishment of a correlation between the drift in FBG peak wavelength of the sensor and the variation in the water content of pork, as depicted in Fig. 11. Through curve fitting, the relationship formula is obtained as follows:

$$\lambda_{\text{simulation}} = 2.535\ 72\mathrm{e}^{-\frac{W}{139.443\ 87}} + 1\ 542.010\ 64. \quad (6)$$

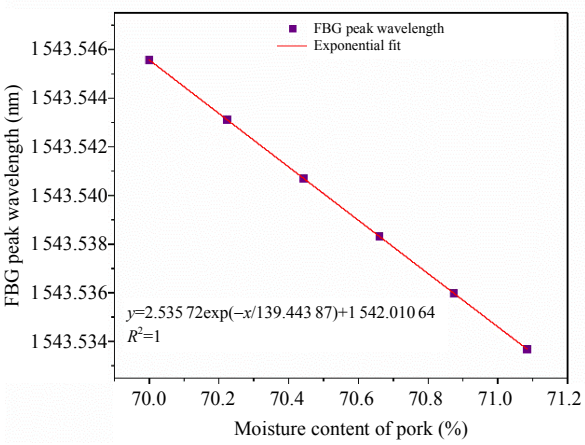

Fig. 11 Practical application model of sensors. In theory, the moisture content of the pork can be measured by the wavelength drift of the FBG sensor.

In this formula, $\lambda_{\text{simulation}}$ is the peak wavelength of the simulated sensor FBG, and the unit is nm; W is the water content of the pork, and the unit is %. Equation (7) is obtained by differentiating (6):

$$\mathrm{d}\lambda = -\frac{2.535\ 72}{139.443\ 87}\mathrm{e}^{-\frac{W}{139.443\ 87}}\mathrm{d}W. \tag{7}$$

In the experiment, the high-resolution OSA used had the resolution of 0.001 nm. When the water content of the pork was W=70%, the sensor was able to detect the minimum change in the water content of the pork using (7), with a sensitivity of dW=0.090 847%.

Comparing experimental and simulation data as shown in Fig. 9(b), it was found that the peak drift of the sensor during the experiment was significantly greater than that predicted by the simulation when injected water ranged from 0 mL to 1.0 mL. However, after injecting 1.0 mL of water, the drift of the FBG peak wavelength was negligible. The analysis suggested that the distribution of water in the pork was not uniform due to factors such as gravity and diffusion, when the water injection position was fixed above the sensor during the experiment. As the sensor was closer to the water injection point, the nearby pork had a relatively higher water absorption rate. Therefore, the sensor detected a higher water content, causing a significant shift in the FBG peak wavelength. After injecting 1.0 mL of water, it became evident that the water content of the pork near the sensor had reached saturation, and the FBG peak wavelength of the sensor was no longer drifting. This method of fixed point and quantitative water injection had the disadvantage of uneven moisture absorption in different parts of the pork sample. But the design of this experiment could verify the sensor's ability to detect the moisture content of the pork. Assuming that the water content of the pork near the sensor reached saturation after injecting 1.0 mL of water, the peak wavelength of the FBG was 1543.529 09 nm. According to (6), the saturated water content of the pork injected with water was approximately 71.505%.

In practice, the moisture content of the injected pork sold in the market is relatively uniform, resulting in consistent detection results that align with the theoretical model.

6. Conclusions

This work proposed a sensor for detecting the meat moisture content, which was based on the photothermal effect of the Er/Yb fiber and the principle of the FBG. It could quantitatively detect the moisture content of the pork after a brief period of heating with pump light. The sensor had the response time of 15 s and could detect changes in the pork moisture content with a sensitivity of 0.090 847%.

The meat moisture content detection sensor proposed in this work had a relatively simple production process and low cost. It could achieve in-situ, rapid, and quantitative detection of the water-injected meat. It is expected to present a novel approach for the swift detection of the water-injected meat.

In the future, portability can be enhanced by researching techniques for integrating on-chip light sources and light detection units. In addition, the water content of the meat varies among different types and cuts, and it is necessary to establish a control group for calibration during the actual testing process. This work only conducted experiments on one type and one part of the pork, and established a mathematical model based on this. Subsequent research can be expanded to cover various types of meat, and corresponding mathematical models can be developed for each type. This will enable the calibration of reference groups during the actual detection process.

Acknowledgment

This work was supported by the National Natural Science Foundation of China (Grant No. 62335010), the Local Innovative and Research Teams Project of Guangdong Pearl River Talents Program (Grant No. 2019BT02X105), the

Fundamental Research Funds for the Central Universities (Grant No. 21623203), and the Guangdong Province College Students Innovation and Entrepreneurship Training Program (Grant No. S202310559031).

Declarations

Conflict of Interest The authors declare that they have no competing interests.

References

[1] Z. Ni, "The reasons and countermeasures for water-injected meat," *Journal of Agricultural Sciences*, 2016, 37(4): 89–92.

[2] W. Zheng, J. Wang, and S. Zhao, "Advances in research of detection techniques for carrageen illegally used in the pre-slaughtering pigs," *China Animal Health Inspection*, 2015, 32(9): 69–71.

[3] L. Cheng, Y. Wang, and S. Lin, "Main hazards and inspection methods of PSE meat, water injected meat and glue injected meat," *Zhejiang Journal Animal Science and Veterinary Medicine*, 2015, 40(3): 13–15.

[4] Z. Tang, Y. Zhou, Y. Zhou, and P. Zheng, "Brief analysis on harm and sensory identification of five kinds of questionable meat," *Meat Industry*, 2015, 12: 47–48.

[5] S. Zhu and C. Li, "Identification and inspection methods of water injected meat," *Technical Advisor for Animal Husbandry*, 2011, 3: 174.

[6] H. Li, "Strengthen the identification and control measures of water injected meat," *Chinese Journal of Veterinary Medicine*, 2013, 49(7): 78–79.

[7] L. Cheng and Y. Jiao, "Inspection methods of the PSE meat，water-injected meat and gel-injected meat," *China Animal Health Inspection*, 2015, 32(4): 28–31.

[8] Y. Huang, G. Chen, J. Xia, and H. Yu, "Status and trends of nondestructive detection technology for water-injected meat," *Transactions of the Chinese Society for Agricultural Machinery*, 2015, 46(1): 207–215.

[9] Y. Leng, Y. Sun, X. Wang, J. Hou, X. Bai, and M. Wang, "A method to detect water-injected pork based on bioelectrical impedance technique," *Journal of Food Measurement and Characterization*, 2019, 13(2): 1341–1348.

[10] S. Gai, Z. Zhang, Y. Zou, and D. Liu, "Rapid and non-destructive detection of water-injected pork using low-field nuclear magnetic resonance (LF-NMR) and magnetic resonance imaging (MRI)," *International Journal of Food Engineering*, 2019, 15(8): 20180313.

[11] H. Yu, J. Xu, H. Liu, C. Liu, D. Zhang, and K. Chen, "Identification of water injection meat based on hyperspectral technique and spectrum characteristics," *Transactions of the Chinese Society for Agricultural Machinery*, 2019, 50(11): 366–372.

[12] J. Liu, Y. Cao, Q. Wang, W. Pan, F. Ma, C. Liu, *et al.*, "Rapid and non-destructive identification of water-injected beef samples using multispectral imaging analysis," *Food Chemistry*, 2016, 190: 938–943.

[13] D. Hao, Y. Zhou, Y. Wang, S. Zhang, Y. Yang, L. Lin, *et al.*, "Recognition of water-injected meat based on vsible/near-infrared spectrum and sparse representation," *Spectroscopy & Spectral Analysis*, 2015, 35(1): 93–98.

[14] M. Wang, L. Xu, L. Chen, S. Hou, G. Wu, and Z. Deng, "A modified soil water content measurement technique using actively heated fiber optic sensor," *Journal of Rock Mechanics and Geotechnical Engineering*, 2020, 12(3): 608–619.

[15] M. Sun, B. Shi, C. Zhang, X. Zheng, J. Guo, Y. Wang, *et al.*, "Quasi-distributed fiber-optic in-situ monitoring technology for large-scale measurement of soil water content and its application," *Engineering Geology*, 2021, 294: 106373.

[16] K. Zhao, H. Gao, F. Chen, R. Wang, and X. Qiao, "Sandy soil moisture content measurement method based on heated fiber Bragg grating," *Optical Fiber Technology*, 2021, 67: 102690.

[17] J. Wang, Z. Li, and J. Wang, "All-optical fiber miniature soil moisture content sensor," *Infrared and Laser Engineering*, 2022, 51(3): 20210299-1–20210299-6.

[18] M. Mehravar, H. Yang, D. J. Webb, W. Zhang, S. F. Sestelani, and D. N. Chapman, "Soil water content measurement using polymer optical fibre Bragg gratings," *Proceedings of the Institution of Civil Engineers – Smart Infrastructure and Construction*, 2021, 174(1): 11–21.

[19] J. Guo, B. Shi, M. Sun, W. Cheng, C. Zhang, G. Wei, *et al.*, "Application of PI-FBG sensor for humidity measurement in unsaturated soils," *Measurement*, 2022, 188: 110415.

[20] M. Sun, B. Shi, C. Zhang, J. Liu, J. Guo, X. Zheng, *et al.*, "Quantifying the spatio-temporal variability of total water content in seasonally frozen soil using actively heated fiber Bragg grating sensing," *Journal of Hydrology*, 2022, 606: 127386.

[21] J. Li, H. Zhu, B. Wu, L. Hu, X. Liu, and B. Shi, "Study on actively heated fiber Bragg grating sensing technology for expansive soil moisture considering the influence of cracks," *Measurement*, 2023, 218: 113087.

[22] Y. Ran, Z. Xu, M. Chen, W. Wang, Y. Wu, J. Cai, *et al.*, "Fiber-optic theranostics (FOT): interstitial fiber-optic needles for cancer sensing and therapy," *Advanced Science*, 2022, 9(15): 2200456.

[23] J. Albert, B. Malo, F. Bilodeau, D. C. Johnson, and M. Kawachi, "Photosensitivity in Ge-doped silica optical waveguides and fibers with 193-nm light from an ArF excimer laser," *Optics Letters*, 1994, 19(6): 387–389.

[24] J. Albert, B. Malo, K. O. Hill, F. Bilodeau, D. C. Johnson, and S. T. Riault, "Comparison of one-photon and two-photon effects in the photosensitivity of germanium-doped silica optical fibers exposed to intense ArF excimer laser pulses," *Applied Physics Letters*, 1995, 67(24): 3529–3531.

[25] P. Xiao, Z. Xu, D. Hu, L. Liang, L. Sun, J. Li, *et al.*, "Efficiently writing Bragg grating in high-birefringence elliptical microfiber for label-free immunosensing with temperature compensation," *Advanced Fiber Materials*, 2021, 3(5): 321–330.

[26] W. Yong, C. Q. Xu, and P. Hong, "Analysis of Raman and thermal effects in kilowatt fiber lasers," *Optics Communications*, 2004, 242(4–6): 487–502.

[27] L. Qi, L. Jin, Y. Liang, L. Cheng, and B. Guan, "Efficiency enhancement of optical tuning for Bragg gratings in rare-earth doped fibers," *IEEE Photonics Technology Letters*, 2014, 26(12): 1188–1191.

[28] M. E. Innocenzi, H. T. Yura, C. L. Fincher, and R. A. Fields, "Thermal modeling of continuous-wave end-pumped solid-state lasers," *Applied Physics Letters*, 1990, 56(19): 1831–1833.

[29] L. Yan and C. H. Lee, "Thermal effects in end-pumped Nd:phosphate glasses" *Journal of Applied Physics*, 1994, 75(3): 1286–1292.

[30] Y. Rong and P. Hu "Thermophysical data of meat," *Meat Industry*, 1996, 2: 42–43.

[31] Y. Deng, "Study on the moisture limit of pork in our country," *Meat Industry*, 2016, 11: 24–27.

[32] D. Sun, Y. Ran, and G. Wang, "Label-free detection of cancer biomarkers using an in-line taper fiber-optic interferometer and a fiber Bragg grating," *Sensors*, 2017, 17(11): 2559.